scientific reports

Check for updates

OPEN

Lead free perovskite integrated metal organic framework as heterogeneous catalyst for efficient three component click reaction

Leila Rezaie Kahkhaie[1], Ali Reza Oveisi[1,2]✉, Esmael Sanchooli[1]✉, Saba Daliran[2] & Mostafa Khajeh[1]

This study reports the synthesis and characterization of a novel $CsCu_2I_3$@UiO-66(Ce)-NH_2 hybrid material through the state-of-the-art in-situ growth of the lead-free and non-toxic $CsCu_2I_3$ perovskite within the porous UiO-66(Ce)-NH_2. The composite exhibits a high surface area with the $CsCu_2I_3$ nanostructures uniformly dispersed within the UiO-66(Ce)-NH_2 framework. The host-guest $CsCu_2I_3$@ UiO-66(Ce)-NH_2 was considered as an effective and stable catalyst for the one-pot three-component copper(I)-catalyzed intermolecular alkyne-azide cycloaddition (CuAAC) or click reaction. Under optimized conditions, utilizing water at room temperature, the nominal catalyst exhibited superior activity, outperforming its individual components. Remarkably, the $CsCu_2I_3$@UiO-66(Ce)-NH_2 catalyst demonstrated good recyclability and reusability over several catalytic runs. Mechanistic studies unveiled a synergistic cooperation between the $CsCu_2I_3$ and MOF, leading to the enhanced catalytic performance and improved stability of the perovskite. The developed multifunctional porous solid offers potential applications in catalysis and related fields, paving the way for innovative and sustainable organic synthesis and beyond.

Keywords Cerium-based metal-organic framework, Composite, Hybrid material, 1,3-Dipolar cycloaddition reaction, Multi-component reaction

Perovskites with the general formula ABX3 have garnered significant attention in recent years as semiconductors due to their remarkable performance in photovoltaic cells and other optoelectronic devices. This is attributed to their unique physical and chemical properties, their simple manufacturing and the ability to tune their characteristics. The most commonly studied perovskites, lead halide perovskites (APbX3), were first reported in the 20th century. However, the materials have limited use due to their poor stability and high toxicity[1–3]. Consequently, extensive research has focused on developing alternative perovskites with lower toxicity and/or higher efficiency.

Cu-based low-dimensional perovskites have shown promise as intrinsic earth-abundant scintillators, exhibiting high photoluminescence quantum yield (PLQY), high thermal stability, and lower toxicity[4,5]. However, the preparation of Cu perovskites faces several challenges, such as the need for capping or stabilizing agents. Additionally, the applications of Cu perovskites have been continuously emerging, but their catalytic performance has not been extensively explored[6–8].

Metal-organic frameworks (MOFs) are another class of heavily studied micro-/mesoporous crystalline materials[9–11]. MOFs are formed by metal ion units or clusters as nodes and organic linkers as connectors. These materials are characterized by their high crystallinity, high specific surface areas (up to 10,000 m^2/g), large internal pore volumes (up to 90% free volume), and low density[12]. Due to these key features, MOFs have been extensively investigated for applications in gas storage/separation[13,14], sensors[15,16], catalysis[17–20], photocatalysis[21], and other areas.

UiO-66(Ce)-NH_2 is an amino-functionalized analog of the well-known UiO-66 MOF[22–24]. This material exhibits several attractive properties, such as exceptional thermal and chemical stability, high porosity, high BET surface area, a relatively simple and mild preparation method, and versatile functionalization capabilities, making it a favorable candidate for various applications[25–27]. The amino groups can serve as anchoring/supporting sites

[1]Department of Chemistry, University of Zabol, P.O. Box: 98615-538, Zabol, Iran. [2]Department of Organic Chemistry, Faculty of Chemistry, Lorestan University, Khorramabad 68151-44316, Iran. ✉email: oveisi.a@lu.ac.ir; aroveisi@uoz.ac.ir; esmael_sanchooli@uoz.ac.ir

for various functional groups, catalysts, or guest molecules, enabling diverse applications such as catalysis, gas storage/separation, and analytical processes[25,28]. Moreover, the incorporation of cerium as the most abundant rare-earth element renders this material a compelling candidate for practical applications[29].

The integration of perovskite and MOF crystals through rational design can result in the formation of a new class of porous composite materials with enhanced structural features, improved stability, higher efficiency and activity rather than using the primary components[6,30–34]. CuAAC or "click" reaction, has been extensively studied for the synthesis of heterocycles used in various field of chemistry, biology, and material science[35,36]. Up to now, $CuSO_4{\cdot}5H_2O/\beta$-cyclodextrin/sodium ascorbate[37], Cu-metallopolymer[38], Cu@UiO-67-IM (IM = imidazolium salt)[39], saCu-x@mpgC_3N_4[40], MOF-derived Cu@N-C[41], and Cu(I) complexes immobilized on multi-walled carbon nanotubes (CNT)[42] have been investigated as CuAAC catalysts. Nevertheless, despite the successful achievements, these systems often suffer from the need for additives or organic solvents, the use of high catalyst amounts, lack of reusability, and long reaction times, which limit their practical applications.

In this work, the hybridization of the cerium-based MOF, UiO-66(Ce)-NH_2, with the lead-free, earth-abundant, and non-toxic $CsCu_2I_3$ perovskite[43–45] to form the $CsCu_2I_3$@ UiO-66(Ce)-NH_2 composite is reported. Using an in-situ growth method, the $CsCu_2I_3$ units are uniformly incorporated within the UiO-66-NH_2 framework, with strong contact between the two components without pore blocking. The UiO-66(Ce)-NH_2 can serve as a nanoscale scaffold, effectively stabilizing and spatially confining the growth of $CsCu_2I_3$ nanostructures, leading to precise control over their size and morphology.

The resulting $CsCu_2I_3$@UiO-66(Ce)-NH_2 composite material was studied as an efficient heterogeneous catalyst for three-component click reaction. The catalytic performance of $CsCu_2I_3$@UiO-66(Ce)-NH_2 surpassed that of its individual components and most reported catalysts. Notably, the $CsCu_2I_3$@UiO-66(Ce)-NH_2 catalyst demonstrated exceptional stability, allowing for facile recovery from the reaction media and efficient reuse without significant loss in catalytic activity. The enhanced catalytic performance was due to a combination effect between the $CsCu_2I_3$ and UiO-66(Ce)-NH_2.

Materials and methods

Chemicals and reagents

Chemical materials such as ammonium cerium(IV) nitrate ($(NH_4)Ce(NO_3)_6$), terephthalic acid (BDC), 2-aminoterephthalic acid (BDC-NH_2), *N*,*N*′-dimethylformamide (DMF), cesium iodide, copper iodide, acetonitrile, sodium azide, benzyl halides, and phenylacetylenes were purchased from Merck and Sigma-Aldrich with high purity. UiO-66(Ce)-NH_2 was prepared according to the previous procedures[22]. Synthesis of individual $CsCu_2I_3$ was adjusted from the literature[43], as mentioned below.

Synthesis of $CsCu_2I_3$

In a glass vial, CuI (1.4 mmol) and CsI (0.70 mmol) were added to anhydrous acetonitrile (5 mL) and stirred for 4 h at 60 °C. The resulting yellow solution underwent controlled cooling to ambient temperature and subsequent filtration through a polytetrafluoroethylene (PTFE) syringe filter (0.45 µm). Subsequently, diethyl ether (approximately 2 mL) was added dropwise as an antisolvent to the filtrate, leading to the formation of a white precipitate of $CsCu_2I_3$. Finally, the crystals were isolated by centrifugation.

Synthesis of UiO-66(Ce)-NH_2

To synthesize UiO-66(Ce)-NH_2, briefly, the process begins by dissolving BDC (70.8 mg, 0.426 mmol) in 2.5 mL of DMF (~ 10 mL glass vial). Then, 800 µL of a 0.533 M solution of $(NH_4)Ce(NO_3)_6$ is added. The vial is sealed, and the mixture is stirred for 30 min at 100 °C. Thee sample is collected *via* centrifugation and washed three times with DMF and ethanol. After the final ethanol wash, the sample is left to soak in ethanol overnight. The solid is then collected by centrifugation, dried under vacuum at 70 °C for 1 h, and activated at 90 °C for 12 h to give UiO-66(Ce). For the solvent-assisted linker exchange (SALE) process, 32.63 mg of UiO-66(Ce), 72.46 mg of BDC-NH_2 (0.4 mmol), and 10 mL of methanol are combined together. The solution is vortexed to ensure thorough mixing, and then sonicated for 5 min, with occasional checks to ensure no sample has settled to the bottom. The sample is then centrifuged and washed with DMF and ethanol, allowing it to soak in the fresh solvent for 30 min during each washing step. The collected sample is then dried under vacuum at 80 °C for 1 h and activated at 40 °C for 24 h.

$CsCu_2I_3$@UiO-66(Ce)-NH_2

The nanostructure was synthesized via antisolvent/inverse solvent infiltration method, following these steps: Copper iodide (CuI, 1.4 mmol) and cesium iodide (CsI, 0.70 mmol) were added to acetonitrile (5 mL) and stirred for 4 h at 60 °C. After cooling the mixture to room temperature, it was filtered through a PTFE filter. The filtered solution was then transferred to a glass vial containing activated UiO-66-NH_2(Ce) (50 mg). The vial was capped and heated at 60 °C for 24 h. Then, the $CsCu_2I_3$ crystals were formed at room temperature by dropwise adding diethyl ether. The reaction was done to get the $CsCu_2I_3$@ UiO-66(Ce)-NH_2 composite. As-synthesized $CsCu_2I_3$@ UiO-66(Ce)-NH_2 composite was filtered and washed by acetonitrile and acetone. The collected crystals were dried in vacuum at 70 °C for 12 h to afford the light brown solid.

Click transformation

Benzyl halide (0.5 mmol), sodium azide (1 mmol), terminal alkyne (1 mmol), and catalyst (10 mg) were combined and stirred in aqueous medium (2 mL). After the completion of the reaction as monitored by TLC (*n*-hexane/ethyl acetate (4:1)), the catalyst was removed by centrifugation. With ethyl acetate the organic phase was extracted. The Na_2SO_4 removes water from the organic extract. Finally, recrystallization from a mixture of ethyl acetate and hexane yielded the pure product.

Reusability of the CsCu2I3@UiO-66(Ce)-NH_2 catalyst

Subsequent to the first run, the catalyst underwent thorough washing with ethyl acetate and acetone. Following the washing step, the catalyst was subjected to drying in an oven maintained at a temperature of 70 °C. Then, the catalyst was reused for the next cycle of the process.

Result and discussion

CsCu2I3@UiO-66(Ce)-NH_2 characterization

Characterization of the $CsCu_2I_3$@Ce-UiO-66-NH_2 composite was carried out using various techniques. PXRD patterns of $CsCu_2I_3$ (Figure S1), UiO-66(Ce) (Figure S2), UiO-66(Ce)-NH_2 and $CsCu_2I_3$@UiO-66(Ce)-NH_2 crystal structures are shown in Fig. 1. As shown in the Fig. 1, the crystallinity of UiO-66(Ce)-NH_2 was remained intact after the growth of $CsCu_2I_3$ crystals. In the hybrid case, the two key peaks at 2θ values of ~7.2° and ~8.3° were observed, matching to (111) and (200) UiO-66 crystal facets[22]. The other characteristic peaks at approximately 12.1°, 17.1°, 22.3°, 25.4°, 25.8°, 29.9°, 34.6°, 35.6°, 43.4°, 43.7°, and 49.7° are respectively assigned to Miller indices of (220), (400), (511), (531), (600), (444), (800), (644), (933), (1000), and (880) of the UiO-66 structure. Notably, the PXRD pattern of the composite exhibits a strong characteristic peak of $CsCu_2I_3$ (PDF#45–0076) at about 43° (440 plan)[46], which overlaps with the 1000 plan of the MOF. This provides a strong evidence for the formation of $CsCu_2I_3$@UiO-66(Ce)-NH_2. The absence of other characteristic peaks of $CsCu_2I_3$ is likely due to its small particle size and low loading amount within the UiO-66(Ce)-NH_2 framework.

Figure 1. PXRD patterns of UiO-66(Ce)-NH_2 (bottom) and $CsCu_2I_3$@UiO-66(Ce)-NH_2 (top). The asterisk corresponds to (440) crystal plane of $CsCu_2I_3$.

In order to check the porosity of the sample, low pressure N_2 adsorption-desorption experiments at 77 K were achieved (Fig. 2a). As depicted in Fig. 2, the N_2 isotherms show a characteristic type I (IUPAC classification), which is an assigned feature of microporous MOFs[47]. The measured Brunauer-Emmett-Teller (BET) surface areas

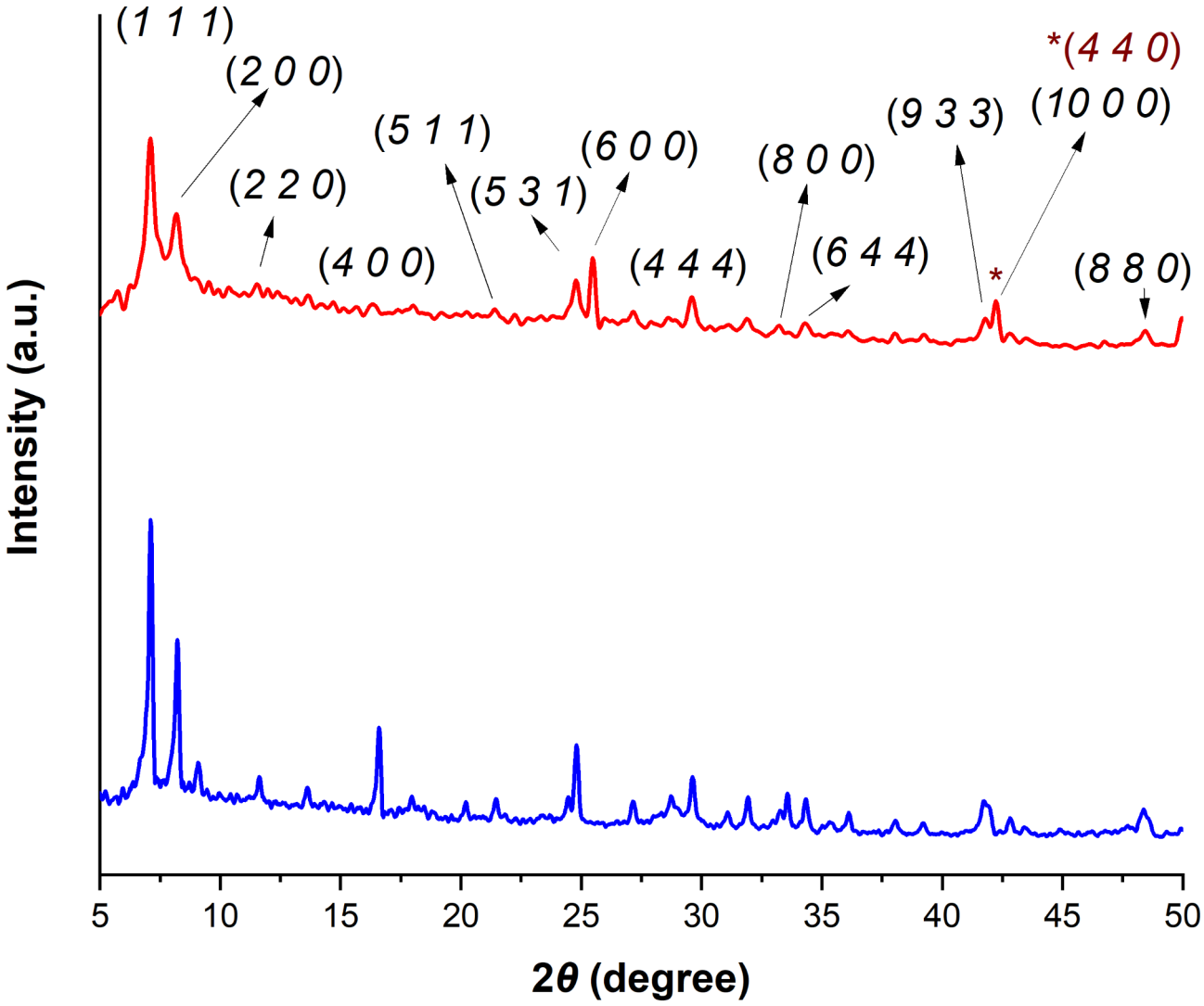

Fig. 1. PXRD patterns of UiO-66(Ce)-NH_2 (bottom) and $CsCu_2I_3$@UiO-66(Ce)-NH_2 (top). The asterisk corresponds to (440) crystal plane of $CsCu_2I_3$.

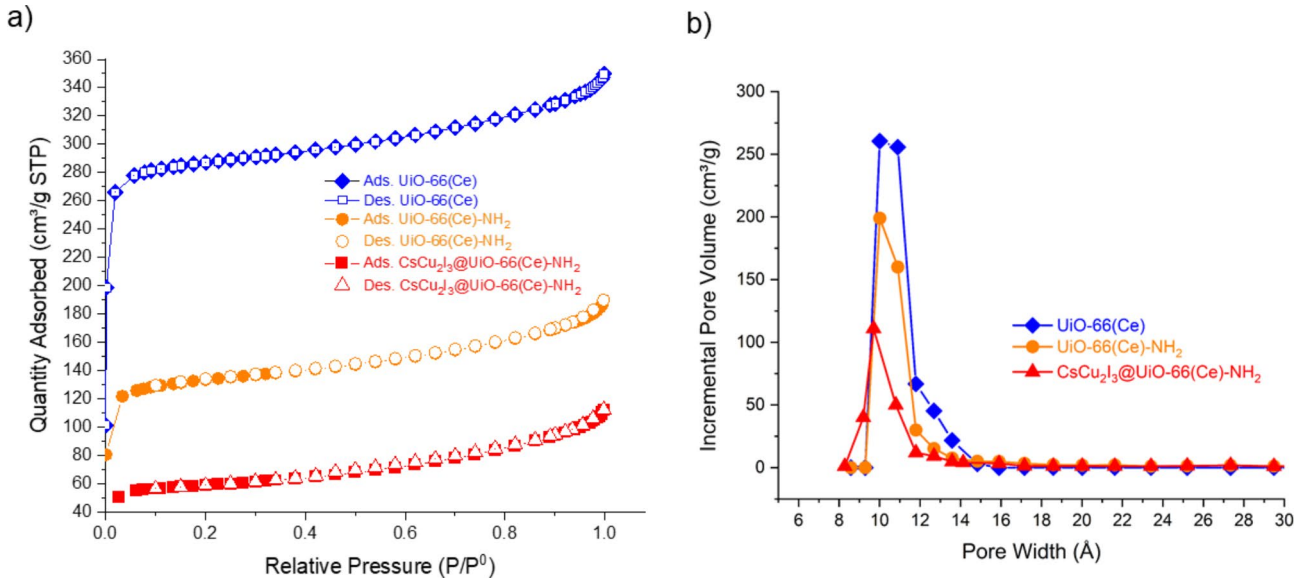

Fig. 2. (**a**) N_2 sorption isotherms of UiO-66(Ce), UiO-66(Ce)-NH_2 and $CsCu_2I_3$@UiO-66(Ce)-NH_2, and (**b**) pore size distributions of the samples.

and pore volume for UiO-66(Ce), UiO-66(Ce)-NH_2 and $CsCu_2I_3$@UiO-66(Ce)-NH_2 samples were calculated to be 850 $m^2\ g^{-1}$ (0.41 cm^3/g), 440 $m^2\ g^{-1}$ (0.15 cm^3/g) and ~200 $m^2\ g^{-1}$ (0.07 cm^3/g), respectively. The observed decreases in surface area and pore volume are attributed to the incorporation of the amino linker and $CsCu_2I_3$, respectively. Additionally, nonlocal density functional theory (NLDFT) pore size distribution (PSD) analysis indicated smaller pore sizes (~0.9 nm) for the $CsCu_2I_3$@UiO-66(Ce)-NH_2 material compared to the parent MOFs (Fig. 2b), further confirming the growth of $CsCu_2I_3$ within the framework.

Figure 2a N_2 sorption isotherms of UiO-66(Ce), UiO-66(Ce)-NH_2 and $CsCu_2I_3$@UiO-66(Ce)-NH_2, and (b) pore size distribution of the different samples.

As shown in Fig. 3, the morphology of the materials was evaluated by FESEM. Accordingly, the $CsCu_2I_3$@UiO-66(Ce)-NH_2 retained the irregular octahedral morphology of the parent UiO-66 interconnected particles, with a size range of 80–300 nm[22]. As a result, the pristine framework is stable as remained undamaged during the composite synthesis.

Figure 3. SEM images of UiO-66(Ce) (a-c), UiO-66(Ce)-NH_2 (d-f), and $CsCu_2I_3$@UiO-66(Ce)-NH_2 (g-i).

Energy-dispersive X-ray (EDS) spectroscopy of $CsCu_2I_3$@UiO-66(Ce)-NH_2 (Figure S3) revealed the following elemental composition (wt%): C (21.68), N (5.33), O (18.37), Cu (0.87), Cs (1.03), and Ce (52.68). The EDS analysis confirmed the formation of $CsCu_2I_3$, showing a Cu/Cs molar ratio of approximately 2:1, consistent with the nominal structure. EDS mapping demonstrated uniform distribution of elements within the framework (Figure S4). Based on the characterization data, $CsCu_2I_3$ primarily forms within the MOF pores rather than as a core-shell structure on the exterior.

X-ray photoelectron spectroscopy (XPS) was performed to confirm the composite formation and to identify the Cu oxidation state in the composite (Figure S5). High-resolution Cu $2p_{3/2}$ spectra of as-synthesized $CsCu_2I_3$@UiO-66(Ce)-NH_2 showed two contributions at 931.2 eV and 933.3 eV, both assigned to Cu(I)[46]. These results suggest that the MOF effectively protects Cu(I) from oxidation to Cu(II) under reaction conditions.

The FT-IR spectra of UiO-66(Ce), UiO-66(Ce)-NH_2, and $CsCu_2I_3$@UiO-66(Ce)-NH_2 provided information about the functional groups present in each material. UiO-66(Ce) is a material with Ce atoms coordinated with BDC organic ligands. Its FT-IR spectrum shows bands corresponding to carboxylate-Ce vibrations at 1547 and 1389 cm^{-1} (Figure S6). UiO-66(Ce)-NH_2 is obtained through a linker exchange method where amine groups as active sites are introduced into the material. The FT-IR spectrum of UiO-66(Ce)-NH_2 shows characteristic bands related to N-H (3420 and 3360 cm^{-1}) and C-N (1259 cm^{-1}) vibrations, indicating the presence of amine groups in the material (Figure S7) [1]. ^{1}H NMR of the digested UiO-66(Ce)-NH_2 approved the linker replacement (Figure S8). For $CsCu_2I_3$, the FT-IR spectrum reveals bands corresponding to the Cs/Cu-I at ~1500–1629 cm^{-1} (Figure S9)[48]. The FT-IR spectrum of $CsCu_2I_3$@UiO-66(Ce)-NH_2 shows a grouping of the characteristic bands of the individual components in the composite material, although with some peak shifts (Figure S10). Significantly, the amino-related peaks of UiO-66(Ce)-NH_2 show reduced intensity and altered positions, suggesting strong interactions with metal ions. These changes provide compelling evidence that the amino groups serve as nucleation sites for the in situ growth of $CsCu_2I_3$ within the MOF structure.

Through careful analysis and comparison with reference spectra of the individual components, one can determine the presence and interactions of the different functional groups and components within the composite material. Thermal gravimetric analysis (TGA) in air demonstrated that the composite exhibits higher thermal stability than both UiO-66(Ce) and UiO-66(Ce)-NH_2 (Figure S11). Mass loss observed below 200 °C is attributed to the removal of solvent trapped in the framework. The data are consistent with the expected characteristics of

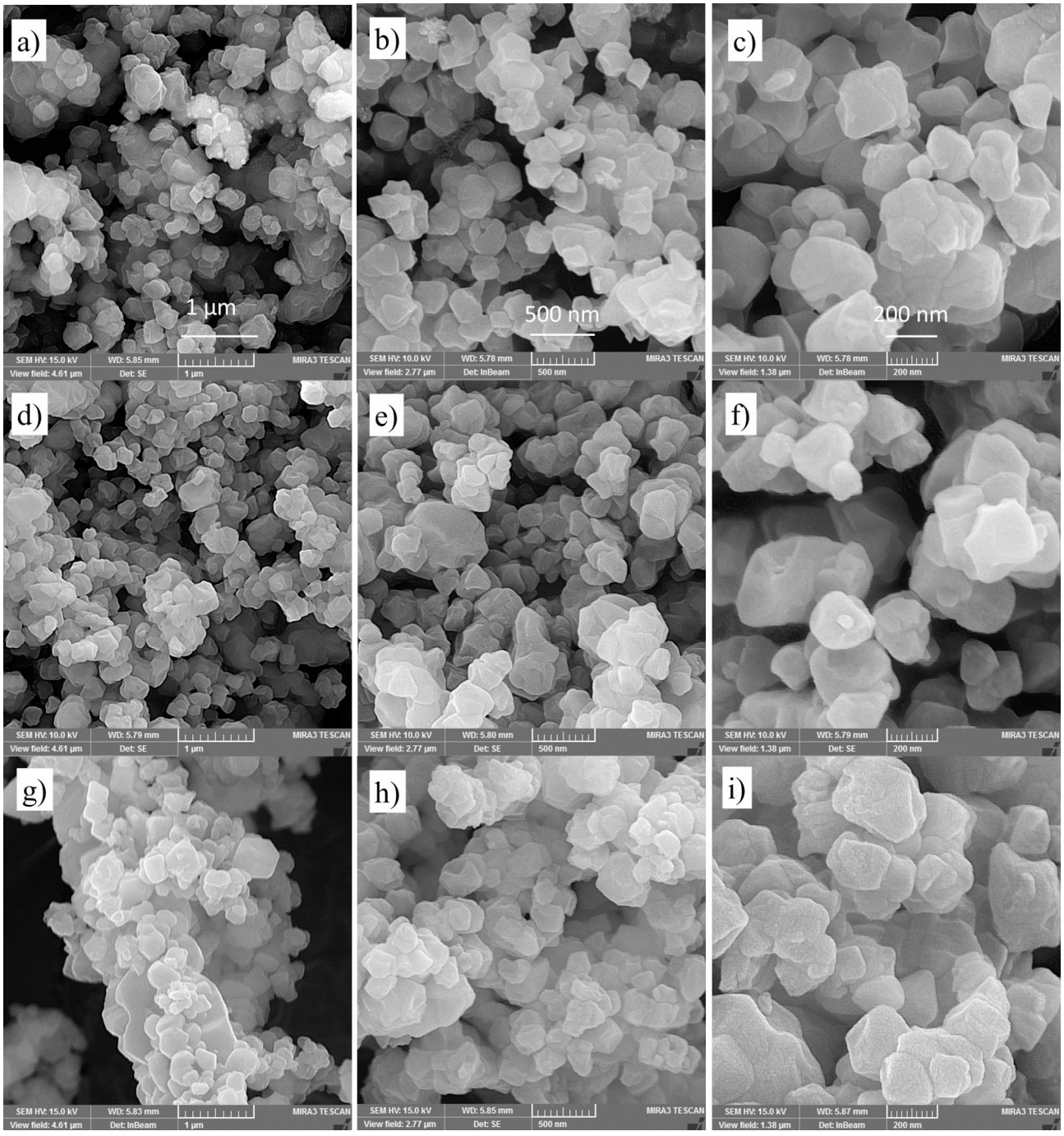

Fig. 3. SEM images of UiO-66(Ce) (**a**–**c**), UiO-66(Ce)-NH_2 (**d**–**f**), and $CsCu_2I_3$@UiO-66(Ce)-NH_2 (**g**–**i**).

such a composite, where the porous UiO-66 provides a high surface area support and the perovskite component contributes to the overall structure and functionality.

Evolution of catalytic activity

To examine the catalytic activity of the $CsCu_2I_3$@UiO-66(Ce)-NH_2, the one-pot three-component CuAAC reaction was investigated. The reaction conditions were optimized using benzyl chloride, sodium azide, and phenylacetylene as the model substrates (Table 1). Table 1 shows the effect of different catalysts, solvents, and temperatures on the CuAAC reaction. The results indicate that water was the most suitable reaction medium as the green solvent, affording the highest yield (90%) of the product in 45 min at room temperature using the $CsCu_2I_3$@UiO-66(Ce)-NH_2 (Table 1, entry 1). The reaction could be also completed within 40 min in water at 50 °C, reaching that of 90% product yield (entry 2). Other solvents, such as ethyl acetate, ethanol, acetonitrile, and ethanol/water resulted in lower yields and longer reaction times (entries 3–6). When the pristine UiO-66-

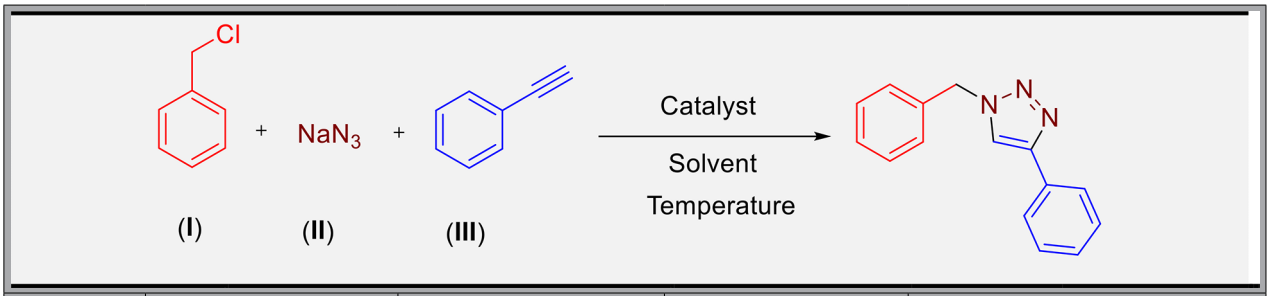

Entry	Solvent	Temperature	Time (min)	Yield (%)[a]
1	H_2O	r.t.	45	90, 87[b], 86[c], 86,[d] 85[e]
2	H_2O	50	40	90
3	EtOAc	r.t.	360	90
4	EtOH	r.t.	45	86
5	CH_3CN	r.t.	480	50
6	H_2O + EtOH	r.t.	45	89
7[f]	H_2O	r.t.	45	–
8[g]	H_2O	r.t.	45	80
9[h]	H_2O	r.t.	60	46
10[i]	H_2O	r.t.	60	–
11[j]	H_2O	r.t.	60	–

Table 1. One-pot three-component CuAAC reaction by different conditions. Reaction conditions: **I** (0.5 mmol), **II** (1 mmol), **III** (1 mmol), solvent (2 mL), and $CsCu_2I_3$@UiO-66(Ce)-NH_2 composite as catalyst (10 mg). [a]Purified yield. [b]The second reused. [c]The third reused. [d]The forth reused. [e]The fifth reused. [f]Pristine UiO-66-NH_2 as catalyst. [g]Individual $CsCu_2I_3$ as catalyst. [h]CuI as catalyst. [i]BDC-NH_2 as catalyst. [j]$(NH_4)Ce(NO_3)_6$ as catalyst.

NH_2 was used as the catalyst (entry 7), no desired product was observed. The $CsCu_2I_3$ (entry 8 *versus* entry 1) also gave a high yield of 80% under the optimum condition, but the catalyst could not be reused effectively. In comparison, the $CsCu_2I_3$@UiO-66(Ce)-NH_2 revealed good recyclability and stability, as evident from entry 1, where the catalyst was reused with only a minimal loss in its catalytic activity after 5 cycles. CuI as catalyst afforded only 46% of product yield (entry 9). BDC-NH_2 and $(NH_4)Ce(NO_3)_6$ precursors as catalysts gave negligible product yield (entries 10 and 11). The composite catalyst demonstrated superior performance compared to individual components, likely due to synergistic effects and improved stability. The composite contains well-dispersed and stable Cu(I) species in the form of $CsCu_2I_3$.

Then, the optimal reaction condition was explored for the synthesis of 1,4-diphenyl-1,2,3-triazole derivatives (Table 2), affording the high yields of 87–92% in 25–70 reaction times with turnover frequencies (TOF) of 272–806 h^{-1}.

The stability of the catalyst was further evaluated by recovering it after being reused through FT-IR (Figure S12), PXRD (Figure S13), SEM (Figure S14), and XPS (Figure S15). The results demonstrated that the recovered catalyst retained its structural, compositional, and morphological features comparable to the fresh catalyst, highlighting its effectiveness and robustness in the reaction. The Cu 2*p* and Ce 3*d* XPS results also suggested that Cu(I) and Ce(IV) are predominant in the composite (Figure S15). In addition, leaching experiment was considered to ensure the integrity of our catalyst system. Atomic Absorption Spectroscopy (AAS) of the filtered reaction solution showed negligible Cu content in the filtered solution (< 0.07 ppm). In addition, UV-Vis spectroscopy of the reaction solution showed no characteristic absorbance peaks of the BDC-NH_2 linker. Furthermore, a hot filtration test was conducted by removing the solid catalyst once the product yield reached 25%. The reaction mixture was monitored for an additional 2 h after catalyst removal, during which no further product formation was observed, confirming the heterogeneous nature of catalysis.

The proposed reaction mechanism, as illustrated in Fig. 4, has been the subject of numerous studies aimed at explaining its pathways[39,40,49–51]. The process begins with the coordination of the alkyne to the Cu(I) center of the $CsCu_2I_3$@UiO-66(Ce)-NH_2, acting as a π-ligand, which consequently enhances the acidity of the C-H bond. After deprotonation, a σ,π-di(copper) acetylide complex (**I**) is succeeded. Simultaneously, the benzyl halide and sodium azide undergo a reaction, generating a benzyl azide intermediate that binds to the Cu(I) center, resulting in the formation of a dicopper intermediate. The acetylide-azide reaction arises *via* an oxidative addition step, yielding a six-membered intermediate (**II**), which subsequently undergoes a reductive elimination process to give the Cu(I)-triazolide intermediate (**III**). The final triazole product is formed through the protonation process, thereby regenerating the catalyst and completing the catalytic cycle. It should be noted that the catalytic activity predominantly occurs within the pores of the composite rather than on its surface. The employed substrates (with Kinetic diameter ~ 1 nm) can diffuse into pores (please see Fig. 2) based on their size. Also, when 9,10-bis(bromomethyl)anthracene was used as a bulker starting material, the reaction yielded negligible product. This observation can settle the size-selective nature of the catalyst.

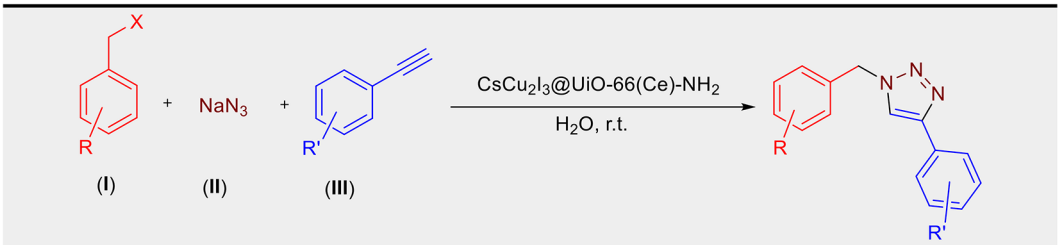

Entry	X	R	R'	Product	Time (min)	Yield (%)[b]	TOF (h^{-1})
1	Cl	H	H	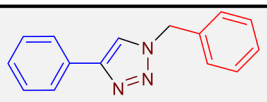	45	90	438
2	Br	H	H	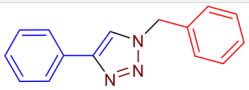	50	92	403
3	Cl	4-NO_2	H	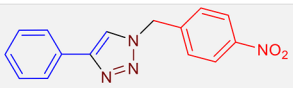	65	90	303
4	Br	4-NO_2	H	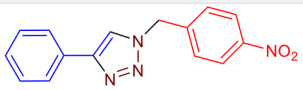	60	90	329
5	Cl	3-NO_2	H	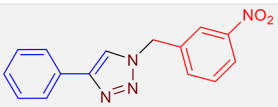	70	87	272
6	Cl	4-NO_2	4-OMe	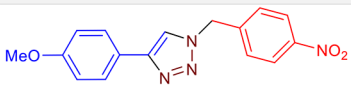	50	91	399
7	Cl	H	4-OMe	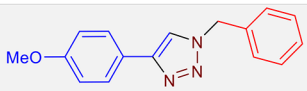	25	92	806

Table 2. One-pot three-component CuAAC reaction by different substrates.
Reaction conditions: **I** (0.5 mmol), **II** (1 mmol), **III** (1 mmol), water (2 mL), and $CsCu_2I_3$@UiO-66(Ce)-NH_2 catalyst (10 mg, 0.87 wt% Cu). [a]Purified yield. [b]TOF = (Number of moles of product formed) / (Number of moles of catalyst × Reaction time).

Figure 4. Suggested reaction pathways of the click reaction over the $CsCu_2I_3$@UiO-66(Ce)-NH_2 catalyst.

Table 3 provides a comparison of the current work (entry 9) with the other reported catalytic systems for three-component click reaction of NaN_3, phenyl acetylene, and benzyl bromide/chloride. The results reveals clearly that the $CsCu_2I_3$@UiO-66(Ce)-NH_2 includes some advantages over the previously reported methods, affording a high product yield (90%) under mild conditions (room temperature, water as the green solvent, and shorter reaction time) and the low dosage of the catalyst with an excellent TOF of 438 h^{-1}.

Conclusion

In this work, a novel $CsCu_2I_3$@UiO-66(Ce)-NH_2 composite was successfully synthesized by incorporating the lead-free and non-toxic $CsCu_2I_3$ perovskite nanostructures within the porous UiO-66(Ce)-NH_2. The catalytic performance of the $CsCu_2I_3$@UiO-66(Ce)-NH_2 was investigated in the one-pot three-component click reaction. The composite catalyst revealed superior activity, affording the desired triazole products in 87–92% yields within 25–70 min (TOFs 272–806 h^{-1}). This catalytic activity outperformed the pristine $CsCu_2I_3$ and UiO-66(Ce)-NH_2 constituents, as well as the most reported catalytic systems. Remarkably, the catalyst exhibited excellent reusability, with minimal loss of activity over multiple catalytic cycles. The developed $CsCu_2I_3$@UiO-66(Ce)-NH_2 hybrid material represents a promising reusable and efficient heterogeneous catalyst for organic transformations, particularly three component click reactions. The synergistic effects arising from the integration of perovskite and MOF components offer opportunities for designing advanced and stable materials with tailored properties and functionalities for various applications in catalysis, photocatalysis, energy, and related fields.

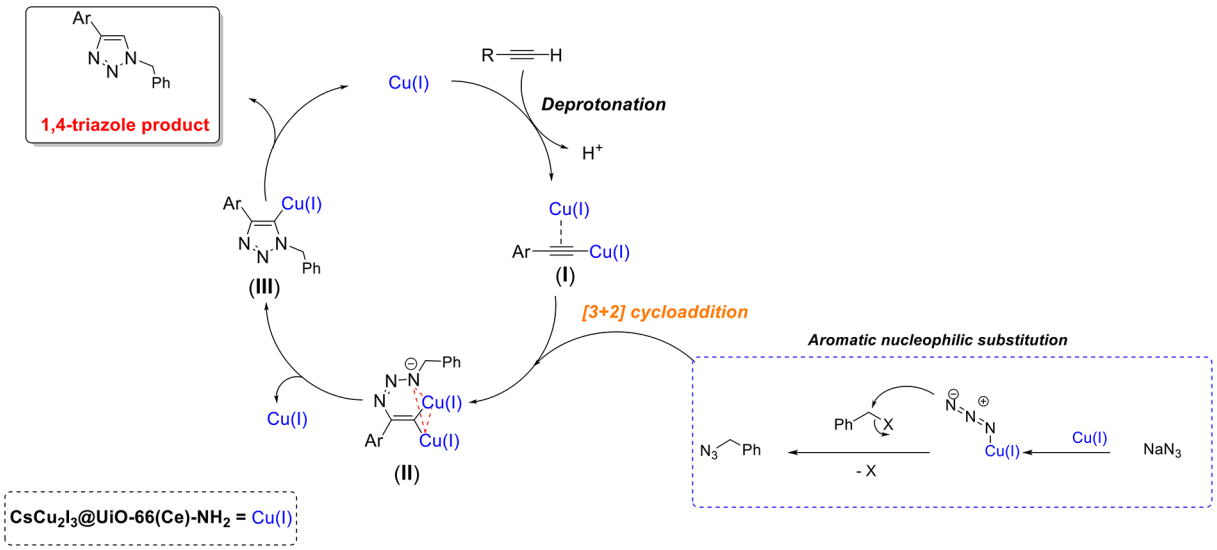

Fig. 4. Suggested reaction pathways of the click reaction over the $CsCu_2I_3$@UiO-66(Ce)-NH_2 catalyst.

Entry	Catalyst or catalytic system (amount)	Solvent	Temperature (°C)	Time (h)	Yield (%)	TOF (h^{-1})	References
1	Cu-metallopolymer (10 mg)[a]	t-BuOH/H_2O	50	2.5	99	66	[38]
2	Cu(I)@UiO-67-IM (1.7 mol%)	H_2O	80	8	68	5	[39]
3	saCu-x@mpgC_3N_4 (30 mg)	H_2O/DMF	130	0.5	45	189	[40]
4	MOF-derived Cu@N-C (10 mg)	t-BuOH/H_2O	50	12	98	0.65	[41]
5	Cu(I) complex immobilized on CNT (5b_CNT-ox-Na) (3 mol%)	H_2O/CH_3CN	MW (30 W, 125 °C)	1	80	26.7	[42]
6	Fe_3O_4@TiO_2/Cu_2O (20 mg)	H_2O	reflux	15 min	93	295	[48]
7	Cu(I)-exchanged solid based on montmorillonite (5 mg)	H_2O	r.t.	2	98	21	[49]
8	$CsCu_2I_3$@UiO-66(Ce)-NH_2 (10 mg; 0.87 wt% Cu ≈ 0.00137 mmol Cu)	H_2O	r.t.	45 min	90	438	This work

Table 3. Comparison of catalytic activity of $CsCu_2I_3$@UiO-66(Ce)-NH_2 with that other catalysts. [a] Assuming 2 wt% Cu

Data availability

The datasets used and analysed during the current study available from the corresponding author on reasonable request.

Received: 28 May 2024; Accepted: 1 January 2025
Published online: 01 March 2025

References

1. Mitzi, D. B. & Introduction: Perovskites *Chem. Rev.* **119**, 3033–3035, (2019).
2. Chowdhury, T. A. et al. Stability of perovskite solar cells: issues and prospects. *RSC Adv.* **13**, 1787–1810 (2023).
3. Du, F. et al. Improving the stability of halide perovskites for photo-, electro-, photoelectro-chemical applications. *Adv. Funct. Mater.* **34**, 2312175 (2024).
4. Yang, S., Tang, Z., Qu, B., Xiao, L. & Chen, Z. Crown-assisted $CsCu_2I_3$ growth and trap passivation for perovskite light-emitting diodes. *ACS Appl. Mater. Interfaces.* **16**, 20776–20785 (2024).
5. Lu, Y., Li, G., Fu, S., Fang, S. & Li, L. $CsCu_2I_3$ nanocrystals: growth and structural evolution for tunable light emission. *ACS Omega.* **6**, 544–552 (2021).
6. Daliran, S., Khajeh, M., Oveisi, A. R., Albero, J. & García, H. $CsCu_2I_3$ nanoparticles incorporated within a mesoporous metal–organic porphyrin framework as a catalyst for one-pot click cycloaddition and oxidation/Knoevenagel tandem reaction. *ACS Appl. Mater. Interfaces.* **14**, 36515–36526 (2022).
7. Tabari, T., Kobielusz, M., Singh, D., Yu, J. & Macyk, W. Cobalt-/Copper-containing perovskites in oxygen evolution and reduction reactions. *ACS Appl. Eng. Mater.* **1**, 2207–2216 (2023).
8. Prašnikar, A., Dasireddy, D. B. C., Likozar, B. & V. & Scalable combustion synthesis of copper-based perovskite catalysts for CO_2 reduction to methanol: reaction structure-activity relationships, kinetics, and stability. *Chem. Eng. Sci.* **250**, 117423 (2022).
9. Xiao, C., Tian, J., Chen, Q. & Hong, M. Water-stable metal–organic frameworks (MOFs): rational construction and carbon dioxide capture. *Chem. Sci.* **15**, 1570–1610 (2024).
10. Gagliardi, L. & Yaghi, O. M. Three future directions for metal–organic frameworks. *Chem. Mater.* **35**, 5711–5712 (2023).
11. Daliran, S. et al. Metal–organic framework (MOF)-, covalent-organic framework (COF)-, and porous-organic polymers (POP)-catalyzed selective C–H bond activation and functionalization reactions. *Chem. Soc. Rev.* **51**, 7810–7882 (2022).

12. Li, D. et al. Advances and applications of Metal-organic frameworks (MOFs) in emerging technologies: a comprehensive review. *Glob Chall.* **8**, 2300244 (2024).
13. Li, Y., Wang, Y., Fan, W. & Sun, D. Flexible metal–organic frameworks for gas storage and separation. *Dalton Trans.* **51**, 4608–4618 (2022).
14. Li, H. et al. Porous metal-organic frameworks for gas storage and separation: Status and challenges. *EnergyChem* 1, 100006, (2019).
15. Kreno, L. E. et al. Metal–organic framework materials as chemical sensors. *Chem. Rev.* **112**, 1105–1125 (2012).
16. Sohrabi, H. et al. Metal-organic frameworks (MOF)-based sensors for detection of toxic gases: a review of current status and future prospects. *Mater. Chem. Phys.* **299**, 127512 (2023).
17. Lee, J. et al. Metal–organic framework materials as catalysts. *Chem. Soc. Rev.* **38**, 1450–1459 (2009).
18. Jiao, L., Wang, J. & Jiang, H. L. Microenvironment modulation in metal–organic framework-based catalysis. *Acc. Mater. Res.* **2**, 327–339 (2021).
19. Dhakshinamoorthy, A., Navalon, S., Asiri, A. M. & Garcia, H. Metal organic frameworks as solid catalysts for liquid-phase continuous flow reactions. *Chem. Commun.* **56**, 26–45 (2020).
20. Oudi, S., Oveisi, A. R., Daliran, S., Khajeh, M. & Teymoori, E. Brønsted-Lewis dual acid sites in a chromium-based metal-organic framework for cooperative catalysis: highly efficient synthesis of quinazolin-(4*H*)-1-one derivatives. *J. Colloid Interface Sci.* **561**, 782–792 (2020).
21. Oudi, S. et al. Straightforward synthesis of a porous chromium-based porphyrinic metal-organic framework for visible-light triggered selective aerobic oxidation of benzyl alcohol to benzaldehyde. *Appl. Catal. A: Gen.* **611**, 117965 (2021).
22. Son, F. A., Atilgan, A., Idrees, K. B., Islamoglu, T. & Farha, O. K. Solvent-assisted linker exchange enabled preparation of cerium-based metal–organic frameworks constructed from redox active linkers. *Inorg. Chem. Front.* **7**, 984–990 (2020).
23. Jacobsen, J., Ienco, A., D'Amato, R., Costantino, F. & Stock, N. The chemistry of Ce-based metal–organic frameworks. *Dalton Trans.* **49**, 16551–16586 (2020).
24. Lammert, M. et al. Cerium-based metal organic frameworks with UiO-66 architecture: synthesis, properties and redox catalytic activity. *Chem. Commun.* **51**, 12578–12581 (2015).
25. Dai, S. et al. Room temperature design of Ce(IV)-MOFs: from photocatalytic HER and OER to overall water splitting under simulated sunlight irradiation. *Chem. Sci.* **14**, 3451–3461 (2023).
26. Armoon, A., Khajeh, M., Oveisi, A. R., Ghaffari-Moghaddam, M. & Rakhshanipour, M. Effective adsorption of methyl orange dye from water samples over copper(II) Schiff-base complex-immobilized cerium-based metal-organic framework. *J. Mol. Struct.* **1304**, 137612 (2024).
27. Ghadim, E. E., Walker, M. & Walton, R. I. Rapid synthesis of cerium-UiO-66 MOF nanoparticles for photocatalytic dye degradation. *Dalton Trans.* **52**, 11143–11157 (2023).
28. Jalalzaei, F., Khajeh, M., Kargar-Shouroki, F. & Oveisi, A. R. Oxime-functionalized cerium-based metal–organic framework for determination of two pesticides in water and biological samples by HPLC method. *J. Nanostructure Chem.* **14**, 95–112 (2024).
29. Shen, C. H. et al. Cerium-based metal–organic framework nanocrystals interconnected by carbon nanotubes for boosting electrochemical capacitor performance. *ACS Appl. Mater. Interfaces.* **13**, 16418–16426 (2021).
30. Cao, J., Tang, G. & Yan, F. Applications of emerging metal and covalent organic frameworks in perovskite photovoltaics: materials and devices. *Adv. Energy Mater.* **14**, 2304027, (2024).
31. Zhang, J. et al. Zr-metal–organic framework based cross-layer-connection additive for stable halide perovskite solar cells. *Appl. Surf. Sci.* **628**, 157339 (2023).
32. Huang, J. N. et al. Efficient encapsulation of $CsPbBr_3$ and au nanocrystals in mesoporous metal–organic frameworks towards synergetic photocatalytic CO_2 reduction. *J. Mater. Chem. A.* **10**, 25212–25219 (2022).
33. Nie, W. & Tsai, H. Perovskite nanocrystals stabilized in metal–organic frameworks for light emission devices. *J. Mater. Chem. A.* **10**, 19518–19533 (2022).
34. Qiao, G. Y. et al. Perovskite quantum dots encapsulated in a mesoporous metal–organic framework as synergistic photocathode materials. *J. Am. Chem. Soc.* **143**, 14253–14260 (2021).
35. Haldón, E., Nicasio, M. C. & Pérez, P. J. Copper-catalysed azide–alkyne cycloadditions (CuAAC): an update. *Org. Biomol. Chem.* **13**, 9528–9550 (2015).
36. Héron, J. & Balcells, D. Concerted cycloaddition mechanism in the CuAAC reaction catalyzed by 1,8-naphthyridine dicopper complexes. *ACS Catal.* **12**, 4744–4753 (2022).
37. Shin, J. A., Lim, Y. G. & Lee, K. H. Copper-catalyzed azide–alkyne cycloaddition reaction in water using cyclodextrin as a phase transfer Catalyst. *J. Org. Chem.* **77**, 4117–4122 (2012).
38. Joshi, S., Yip, Y. J., Türel, T., Verma, S. & Valiyaveettil, S. Cu–tetracatechol metallopolymer catalyst for three component click reactions and β-borylation of α,β-unsaturated carbonyl compounds. *Chem. Commun.* **56**, 13044–13047 (2020).
39. Hu, Y. H., Wang, J. C., Yang, S., Li, Y. A. & Dong, Y. B. CuI@UiO-67-IM: a MOF-based bifunctional composite triphase-transfer catalyst for sequential one-pot azide–alkyne cycloaddition in water. *Inorg. Chem.* **56**, 8341–8347 (2017).
40. Vilé, G. et al. Azide-alkyne click chemistry over a heterogeneous copper-based single-atom catalyst. *ACS Catal.* **12**, 2947–2958 (2022).
41. Wang, Z., Zhou, X., Gong, S. & Xie, J. MOF-derived Cu@N-C catalyst for 1,3-dipolar cycloaddition reaction. *Nanomaterials* **12**, 1070 (2022).
42. Librando, I. L. et al. Synthesis of a bovel series of Cu(I) complexes bearing alkylated 1,3,5-triaza-7-phosphaadamantane as homogeneous and carbon-supported catalysts for the synthesis of 1- and 2-substituted-1,2,3-triazoles. *Nanomaterials* **11**, 2702 (2021).
43. Li, Y. et al. Solution-processed one-dimensional $CsCu_2I_3$ nanowires for polarization-sensitive and flexible ultraviolet photodetectors. *Mater. Horiz.* **7**, 1613–1622 (2020).
44. Lin, R. et al. All-inorganic $CsCu_2I_3$ single crystal with High-PLQY (≈ 15.7%) intrinsic white-light emission via strongly localized 1D excitonic recombination. *Adv. Mater.* **31**, 1905079 (2019).
45. Yan, S. S. et al. Enhanced optoelectronic performance induced by ion migration in lead-free $CsCu_2I_3$ single-crystal microrods. *ACS Appl. Mater. Interfaces.* **14**, 49975–49985 (2022).
46. Mo, X. et al. Highly-efficient all-inorganic lead-free 1D $CsCu_2I_3$ single crystal for white-light emitting diodes and UV photodetection. *Nano Energy.* **81**, 105570 (2021).
47. Oveisi, A. R., Daliran, S. & Peng, Y. in *Catalysis in Confined Frameworks* (eds Garcia H. & Dhakshinamoorthy A.) Ch. 3, 97–126, Wiley, (2024).
48. Archana, K. M., Yogalakshmi, D. & Rajagopal, R. Application of green synthesized nanocrystalline CuI in the removal of aqueous Mn(VII) and Cr(VI) ions. *SN Appl. Sci.* **1**, 522, (2019).
49. Nemati, F., Heravi, M. M. & Elhampour, A. Magnetic nano-Fe_3O_4@TiO_2/Cu_2O core–shell composite: an efficient novel catalyst for the regioselective synthesis of 1,2,3-triazoles using a click reaction. *RSC Adv.* **5**, 45775–45784 (2015).
50. Mekhzoum, M. E. M., Benzeid, H., Qaiss, A. E. K., Essassi, E. M. & Bouhfid, R. Copper(I) confined in interlayer space of montmorillonite: a highly efficient and recyclable catalyst for click reaction. *Catal. Lett.* **146**, 136–143 (2016).
51. Ayouchia, B. E., Bahsis, H., Anane, L., Domingo, H., Stiriba, S. E. & L. R. & Understanding the mechanism and regioselectivity of the copper(I) catalyzed [3 + 2] cycloaddition reaction between azide and alkyne: a systematic DFT study. *RSC Adv.* **8**, 7670–7678 (2018).

Acknowledgements
This work has been funded by the University of Zabol (Grant numbers: UOZ-GR-8175, UOZ-GR-9381, and UOZ-GR-4188). Authors also thank the Lorestan University for the support.

Author contributions
L.R.K., A.R.O., E.S., S.D., and M.K. considered the experiments presented herein. L.R.K. synthesized and characterized the catalyst under supervision of S.D. and E.S. The organic reactions carried out by L.R.K. A.R.O. and E.S. supervised the project. S.D. and M.K. wrote the initial draft of the paper with inputs and corrections from all co-authors. A.R.O. E.S. and S.D. finalized the manuscript.

Declarations

Competing interests
The authors declare no competing interests.

Additional information
Supplementary Information The online version contains supplementary material available at https://doi.org/10.1038/s41598-025-85204-x.

Correspondence and requests for materials should be addressed to A.R.O. or E.S.

Reprints and permissions information is available at www.nature.com/reprints.

Publisher's note Springer Nature remains neutral with regard to jurisdictional claims in published maps and institutional affiliations.